JOURNAL OF MATERIALS SCIENCE 37 (2002) 3925–3933

Yttrium implantation effect on 304L stainless steel high temperature oxidation at 1000°C

F. RIFFARD *,‡, H. BUSCAIL, E. CAUDRON, R. CUEFF, C. ISSARTEL, S. PERRIER
Laboratoire Vellave sur l'Elaboration et l'Etude des Matériaux, Equipe Locale Université Blaise Pascal Clermont-Fd II, B.P. 219, 43006 Le Puy en Velay, France
E-mail: Riffard@iut.u-clermont1.fr

Scanning electron microscopy (SEM), energy dispersive X-ray spectrometry (EDXS) and *in situ* X-ray diffraction techniques were carried out to observe the oxide scale evolutions of yttrium implanted and unimplanted commercial 304L stainless steels during and after their high temperature oxidation at 1000°C for 100 h. Our results clearly demonstrate that yttrium implantation promotes a faster oxide scale growth and the formation of a more uniform chromia layer due to a higher chromium selective oxidation compared to unimplanted 304L stainless steel. Moreover, the presence of yttrium also leads to the formation of an enriched silicon layer at the metal-oxide interface limiting the growth of iron-based oxides which were not detected (even during cooling) in the case of yttrium implanted samples. These results allow to understand the low weight gain of yttrium implanted 304L stainless steel observed by thermogravimetry and underline the beneficial effect of yttrium implantation on the 304L oxidation resistance at high temperature.

1. Introduction

It is now well established that small additions (<1%) of oxygen reactive elements such as cerium, yttrium or hafnium into iron alloys allow improvement of their oxidation resistance at high temperature [1–15]. These elements added to the bulk alloy or to the surface are able, in particular, to dramatically improve the oxide scale adherence and to decrease the iron alloy oxidation rate at high temperature. However, the underlying mechanisms of the reactive element effect are still the subject of discussion. In fact, under high temperature oxidizing conditions, the presence of oxygen reactive elements promotes the formation of a protective and more compact thin layer near the iron alloy surface. Moreover, this thin layer is very adherent to the iron alloy even under thermal cycling oxidation. In the case of chromia-forming alloys several authors [2, 4–6, 9, 13] have clearly demonstrated that the presence of yttrium induces an inversion of the predominant diffusion process (inward anionic diffusion instead of outward cationic diffusion generally observed in the case of chromia-forming alloy) due to the blocking of short circuit diffusion paths (e.g., grain boundaries) by yttrium segregation into these grain boundaries. Some authors [2, 3, 9] have also shown that yttrium incorporation into the bulk of chromia-forming alloy improves the oxide scale adherence by limiting the growth of pores at the metal-oxide interface. Moreover, the formation of a continuous protective oxide layer is obtained with very low yttrium concentrations. The other main beneficial effects attributed to yttrium incorporation into chromia-forming alloys are respectively: (a) the reduction of the internal oxide layer stresses ; (b) an enhanced selective oxidation of chromium [2, 3, 9]; (c) the formation of a fine-grain oxide layer [2, 4–10, 14].

The aim of this study is to observe the yttrium implantation effect on the high temperature oxidation resistance of a commercial chromia-forming alloy (i.e., 304L stainless steel). This work constitutes in fact the next stage of our study concerning the understanding of the yttrium implantation effect on steel oxidation resistance at high temperature [15].

2. Experimental procedure

Coupons of 304L grade steel specimens (Fe: 70.51%; Cr: 17.9%; Ni: 9.05%; Mn: 1.52%; Si: 0.48%; Co: 0.22%; Mo: 0.15%; Cu: 0.1%; C: 0.05%; Ti: 0.01%; S: 0.01% in weight obtained using inductively coupled plasma mass spectrometry (ICPMS)) of 3 cm^2 total area and thickness 2 mm were cut from cold-rolled plates. These samples were abraded with up to 800-grit SiC paper, degreased with ethanol and dried. This surface preparation is followed by yttrium implantation (corresponding to a nominal dose of 10^{17} ions/cm^2) carried out by sample surface scanning using a 0.5 mm ion beam diameter (acceleration potential: 180 kV—current: 30–35 mA) to obtain the whole surface implantation on the two main coupon faces.

*Author to whom all correspondence should be addressed.
‡*Present Address*; Laboratoire Vellave sur l'Elaboration et l'Etude des Matériaux, Institut Universitaire de Technologie, Département de Chimie-Science des Matériaux, 8 rue J.B Fabre, B.P. 219, 43006 Le Puy en Velay, France.

Isothermal weight gain measurements were carried out by thermogravimetry (TGA) using a TG-DTA 92-1600 Setaram microthermobalance for 100 h at 1000°C in air. The characterization of the sample oxidation was performed by *in situ* X-ray diffraction, scanning electron microscopy (SEM) and energy dispersive X-ray spectrometry (EDXS). *In situ* X-ray diffraction studies were performed every hour using a high temperature Anton PAAR HTK 1200 chamber with an integrated sample spinner in a Philips X'pert MPD diffractometer equipped with a curved Cu monochromator (Cu $K_{\alpha 1} = 0.1540560$ nm radiation). The most representative *in situ* X-ray spectra only will be presented in this paper.

3. Results and discussion

3.1. Oxidation kinetics at high temperature

Fig. 1 shows the weight gain per cm^2 versus time curves ($\Delta m/S = f(t)$) of yttrium implanted and unimplanted samples oxidized for 100 h at 1000°C in air (atmospheric pressure). The weight gain curve of non-treated 304L steel oxidized sample exhibits two different parts: A first 10-h transient linear regime corresponding to a significant weight gain (0.5 mg/cm^2) which is characteristic of a layer not completely established followed by a pseudo-parabolic behavior according to Wagner's law up to the end of the oxidation test. This latter behavior is characteristic of an oxidation rate limited by the diffusion of one or more species through a compact layer increasing in thickness (parabolic rate constant: $k_{p(blank)} = (2.9 \pm 0.2)10^{-12}\ g^2 \cdot cm^{-4} \cdot s^{-1}$). The resulting weight gain, after 100-h oxidation test, is about 1.26 mg/cm^2.

By contrast, yttrium implanted specimen exhibits directly a parabolic weight gain curve (parabolic rate constant: $k_{p(Y-implanred)} = (0.32 \pm 0.02)10^{-12}\ g^2 \cdot cm^{-4} \cdot s^{-1}$) throughout the oxidation test (no initial transient stage was observed). Moreover, after the 100-h oxidation test, the resulting weight gain (0.35 mg/cm^2) is lower than in the case of unimplanted sample. These results underline the beneficial effect of the yttrium implantation which avoids the presence of the initial transient stage and allows enables reduction of the parabolic rate constant (by a factor 9).

3.2. *In situ* high temperature X-ray diffraction studies

3.2.1. Isothermal 304L stainless steel oxidation

The initial 304L steel (austenitic steel (JCPDS 33-397)) and the *in situ* high temperature main XRD experimental spectra obtained during the first 24-h sample oxidation are shown in Fig. 2 (no significant XRD spectra changes are observed after the first 24 h). *In situ* high temperature diffraction analyses reveal the initial nucleation stage of (Cr_2O_3) chromia (JCPDS 38-1479) and the formation of a spinel oxide $Mn_{1.5}Cr_{1.5}O_4$ (JCPDS 33-892) at the beginning of the oxidation test. The evolution of the characteristic diffraction peak intensities of the induced oxides and metallic substrate during the first 8-h underlines the formation of a layer at the oxide-gas interface by external diffusion of the Mn^{2+} and Cr^{3+} cations. After the first 8-h oxidation test, the oxide scale becomes sufficiently thick to mask the substrate characteristic diffraction peaks and two new compounds (i.e., hematite: α-Fe_2O_3 (JCPDS 33-664) and another spinel oxide $FeCr_2O_4$ (JCPDS 34-140)) are also observed. However, it is interesting to note that some characteristic diffraction peaks of Fe_2O_3 and Cr_2O_3 could also correspond to the compound $Fe_{1.2}Cr_{0.8}O_3$ (JCPDS 34-412) which is a solid solution of hematite and chromia as indicated by the Fe_2O_3-Cr_2O_3 phase diagram [19]. These results suggest the formation of an oxide scale in which the initial transient nucleation stage corresponds to the nucleation of a protective chromia scale with small amounts of spinel oxides. The linear rate law observed by thermogravimetry can be attributed to the presence of the spinel oxide implying the formation of an initial non-uniform protective chromia scale. The evolution of the oxide characteristic X-ray diffraction peak intensities seems to suggest the formation of a multi-layer structure constituted by an internal chromia and Mn,Cr-spinel oxide scale and by an external scale of iron oxides (i.e., α-Fe_2O_3 and $FeCr_2O_4$).

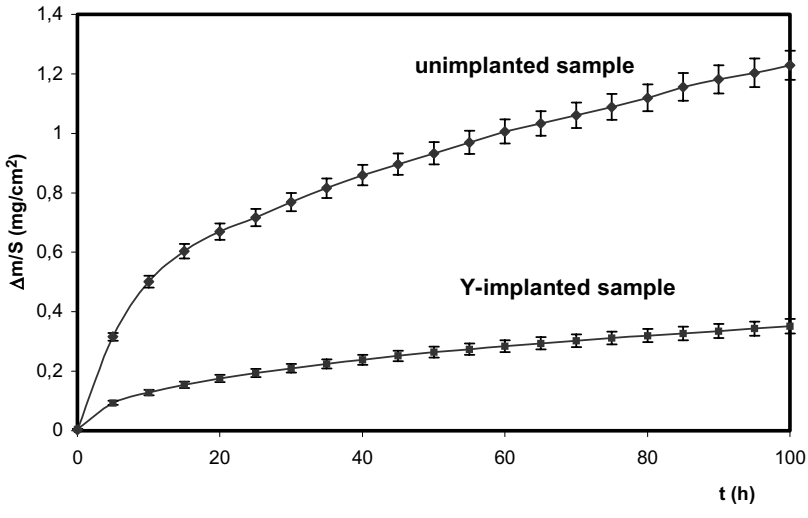

Figure 1 Thermogravimetric studies of the reference and yttrium implanted 304L stainless steels (100 h at $T = 1000$°C in air).

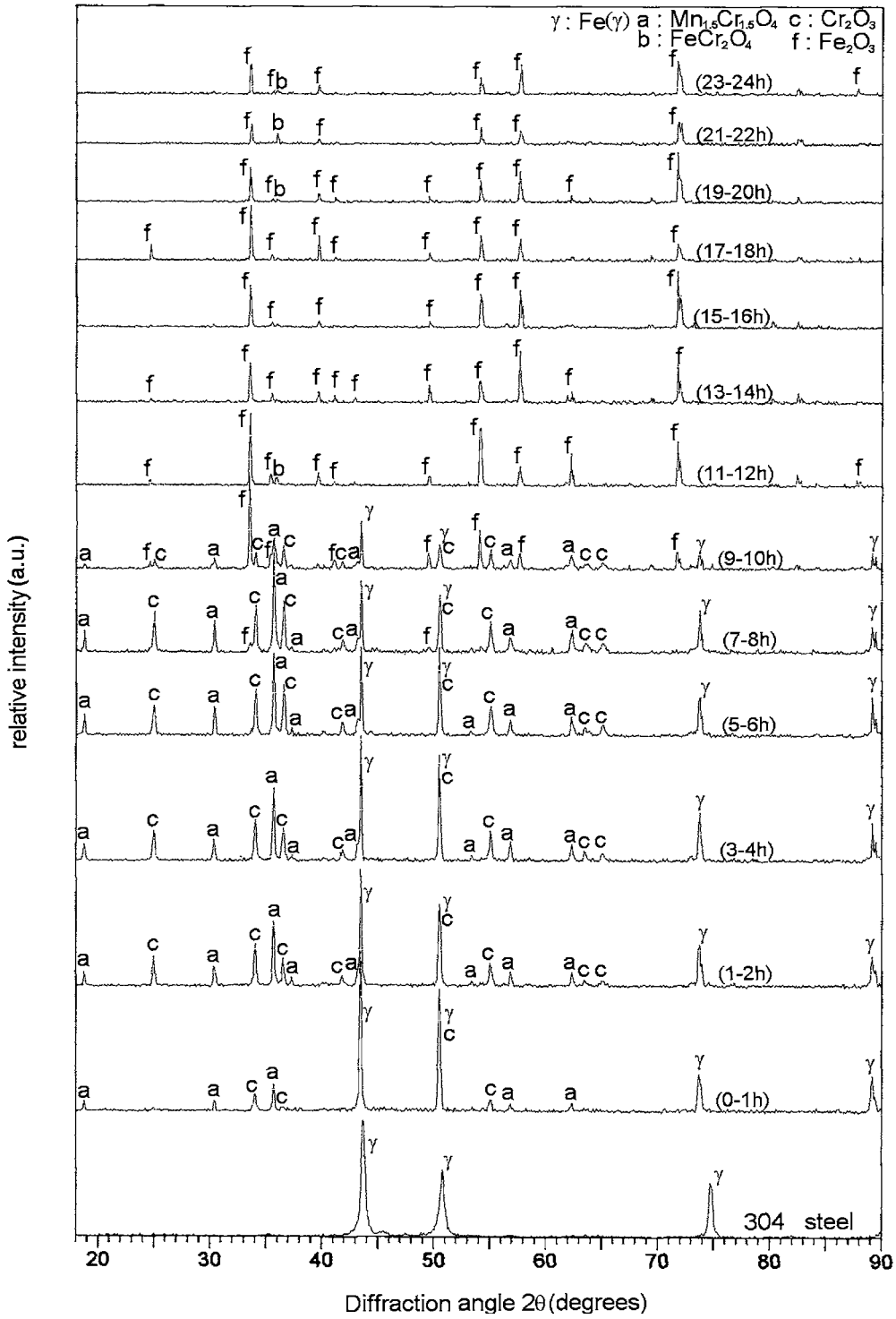

Figure 2 Initial sample and *in situ* high temperature XRD experimental spectra performed on unimplanted 304L stainless steel showing the main structures induced during formed a high temperature oxidation test ($T = 1000°C$ in air).

In fact, the formation of the external $FeCr_2O_4$ compound can be explained by the reaction between Cr_2O_3 and FeO induced by our high temperature experimental conditions.

3.2.2. Isothermal yttrium implanted 304L stainless steel oxidation

Fig. 3 shows the initial yttrium implanted stainless steel sample (before oxidation) and the most representative *in situ* high temperature XRD spectra performed during the first 24-h oxidation test (no significant XRD spectra evolution is observed after the first 24 h as in the case of unimplanted steel). The most interesting result is the fact that Cr_2O_3 (JCPDS 38-1479) and $Mn_{1.5}Cr_{1.5}O_4$ (JCPDS 33-892) are the only main compounds promoted by the oxidation test. In fact, iron or yttrium oxide characteristic diffraction peaks are not detected during *in situ* high temperature X-ray diffraction analyses and the resulting oxide scale was sufficiently thin to observe the substrate characteristic diffraction peaks (JCPDS 33-397) throughout the oxidation test. Yttrium implantation seems to promote the rapid formation of a compact oxide scale (as suggested by the parabolic oxidation rate observed by thermogravimetry) constituted by Cr_2O_3 and $Mn_{1.5}Cr_{1.5}O_4$. Similar results are obtained by some authors [16–22] showing that yttrium

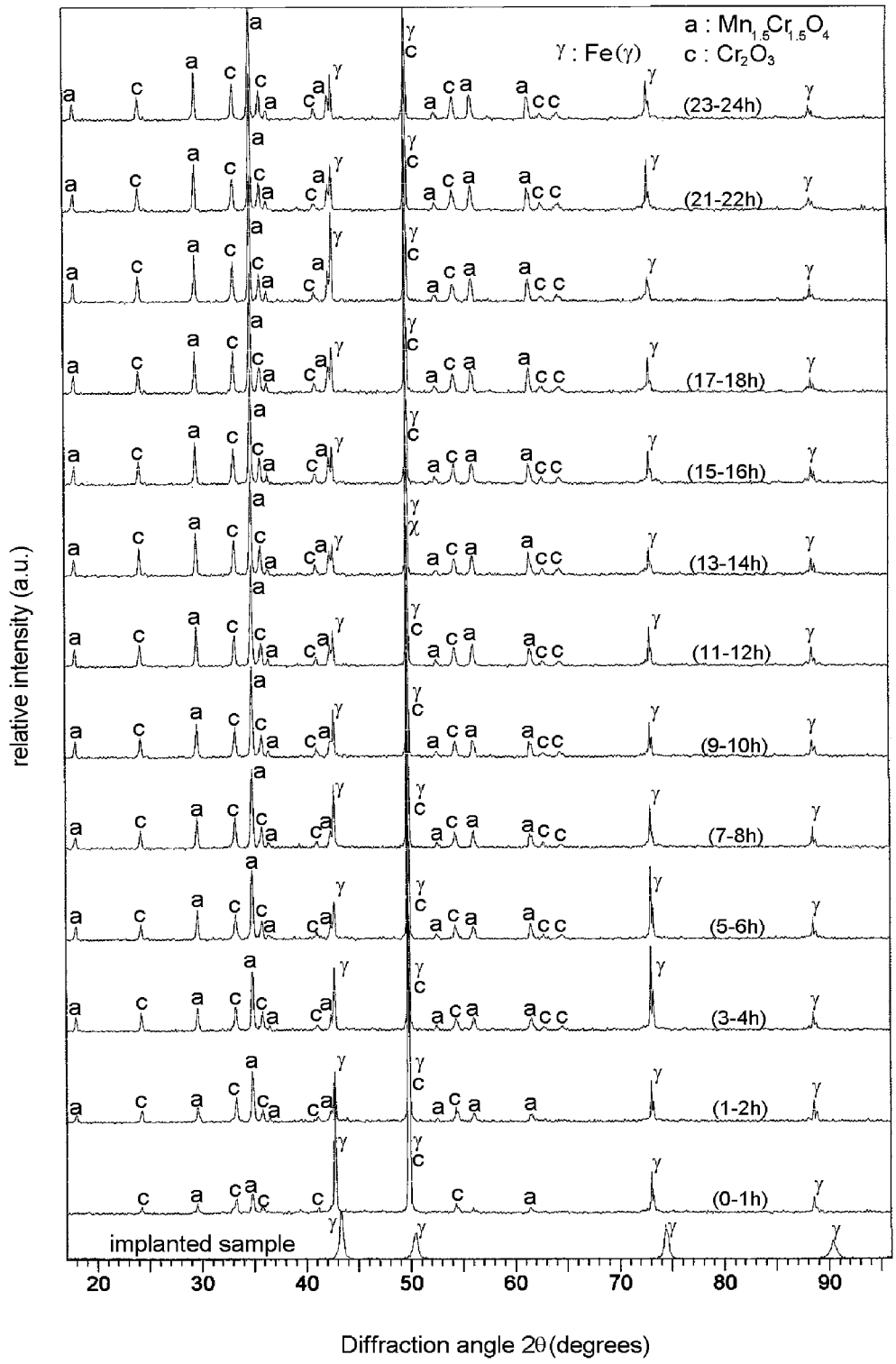

Figure 3 Initial sample and *in situ* high temperature XRD experimental spectra performed on yttrium implanted 304L stainless steel showing the main structures induced during a high temperature oxidation test ($T = 1000°C$ in air).

implantation induces the formation of Cr_2O_3 fine grains with yttrium segregation at the oxide grain boundaries.

3.3. *In situ* X-ray diffraction characterization of the oxide scale during cooling

After the high temperature oxidation test, the samples were cooled down to room temperature by stages of 200°C inside the diffractometer high temperature chamber. X-ray analyses performed on unimplanted 304L stainless steel (Fig. 4) clearly shows the external oxide scale constituted only by Fe_2O_3 and $FeCr_2O_4$ compounds. By contrast, only the Cr_2O_3 and $Mn_{1.5}Cr_{1.5}O_4$ compounds were detected during the cooling of yttrium implanted 304L stainless steel (Fig. 5).

3.4. Oxide scale characterization after cooling

After cooling, the oxide scale was mainly characterized by two techniques: scanning electron microscopy (SEM) and energy dispersive X-ray spectrometry (EDXS). In order to observe the oxide layers,

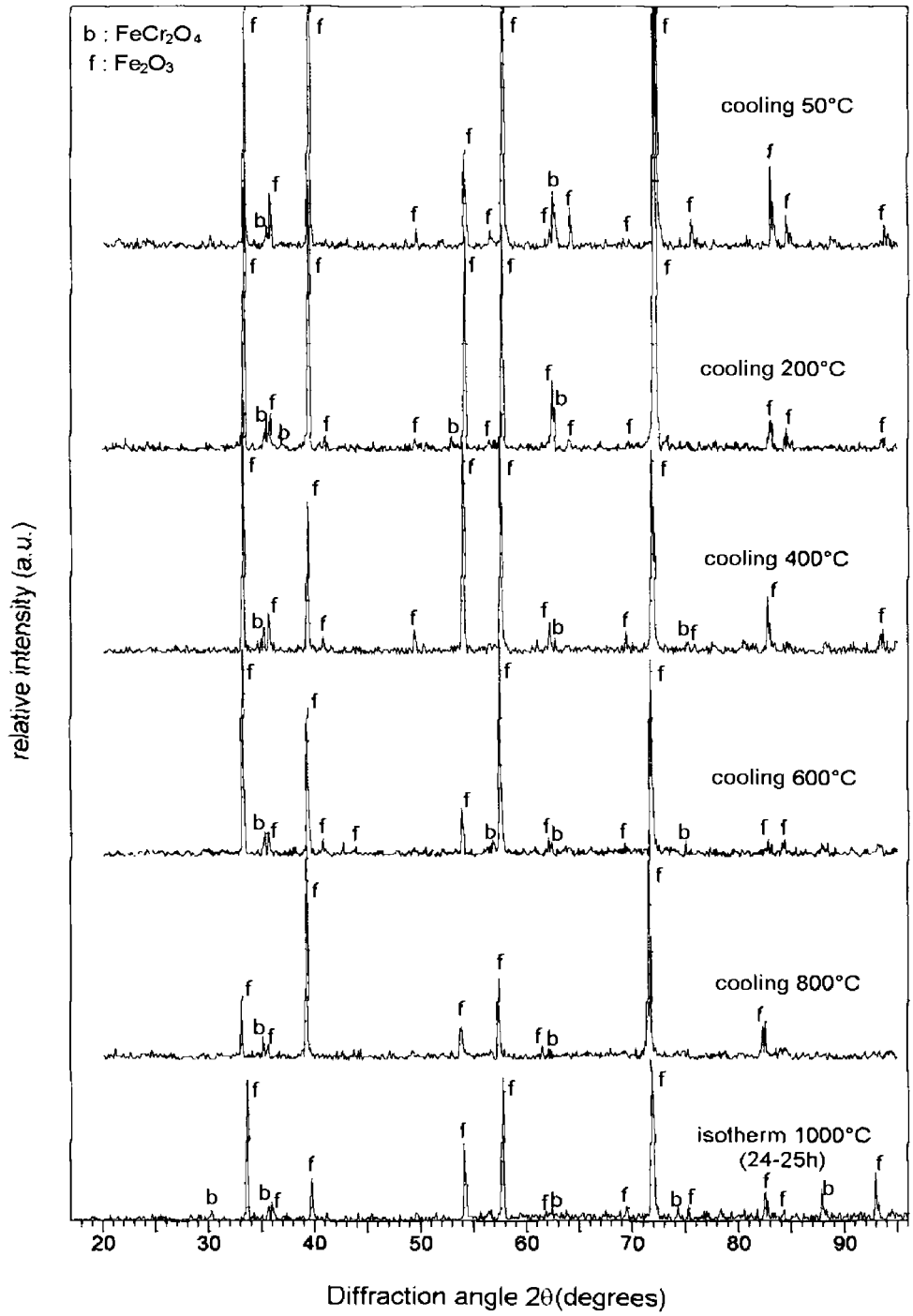

Figure 4 In situ XRD experimental spectra performed during the cooling of the 304L reference stainless steel (after a 100-h high temperature oxidation test at 1000°C in air).

their cross-sections were prepared after copper electrodeposition to preserve the scale during polishing. SEM micrographs of both sample cross-sections after 100-h oxidation tests (Fig. 6) allow determination of the mean oxide scale thicknesses which are respectively (6 ± 2) μm for the unimplanted sample and (2.5 ± 0.4) μm for the yttrium implanted sample. However, the estimation of the oxide layer mean thickness is difficult, especially in the case of unimplanted sample, because of non-regular oxide scale formations as shown in Fig. 6. Comparison of SEM and thermogravimetric results clearly shows significant differences for both yttrium implanted and unimplanted samples which can be explained by a surface layer spallation phenomenon occurring during the sample cooling (vertical sample disposition in the TGA microthermobalance).

3.4.1. EDXS analyses of cooled unimplanted 304L stainless steel

EDXS analyses of the unimplanted sample cross-section (Fig. 7) reveal the presence of silicon in small amounts near the metal-oxide interface in addition to chromium oxide. Iron and manganese enrichments near the oxide-gas interface are also detected indicating important manganese and iron external diffusion which confirms the presence of $Mn_{1.5}Cr_{1.5}O_4$, Fe_2O_3 and $FeCr_2O_4$ compounds identified by *in situ* X-ray diffraction.

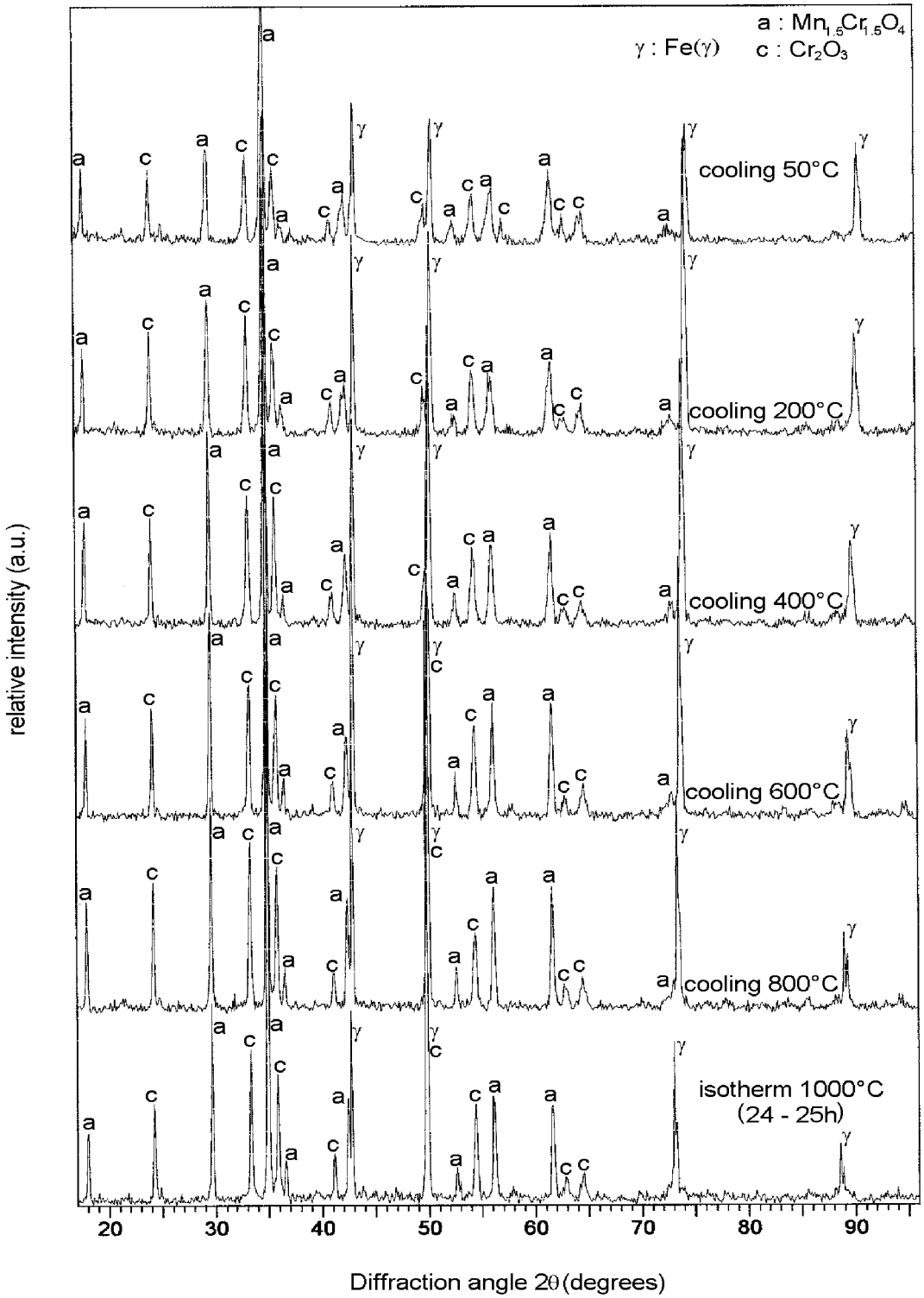

Figure 5 In situ XRD experimental spectra performed during the cooling of the 304L yttrium implanted stainless steel (after a 100-h high temperature oxidation test at 1000°C in air).

3.4.2. EDXS analyses of cooled yttrium implanted 304L stainless steel

EDXS analyses (Fig. 8) clearly show that yttrium is mainly localized at the metal-oxide interface even if no yttrium compounds were detected by X-ray diffraction (probably because of yttria nanocrystalline phase concentrations below the detection limit of our XRD equipment). However, some authors [5, 6, 14, 16–22] have demonstrated that yttrium segregates at the oxide grain boundaries in form of $YCrO_3$ nanocrystalline phases promoting a selective chromium oxidation and consequently the rapid formation of the protective chromia layer. Interestingly enough, some studies [5, 6, 14] clearly indicate that the presence of $YCrO_3$ compound at the oxide grain boundaries induces an inversion of the predominant diffusion mechanism (anionic internal diffusion instead of external cationic diffusion). Fig. 8 also underlines a more important silicon enrichment (mainly localized at the oxide-metal interface and inside the metal substrate) than in the case of unimplanted sample. This phenomenon was also observed by some authors [8] in the case of the AISI 304L chromia-forming

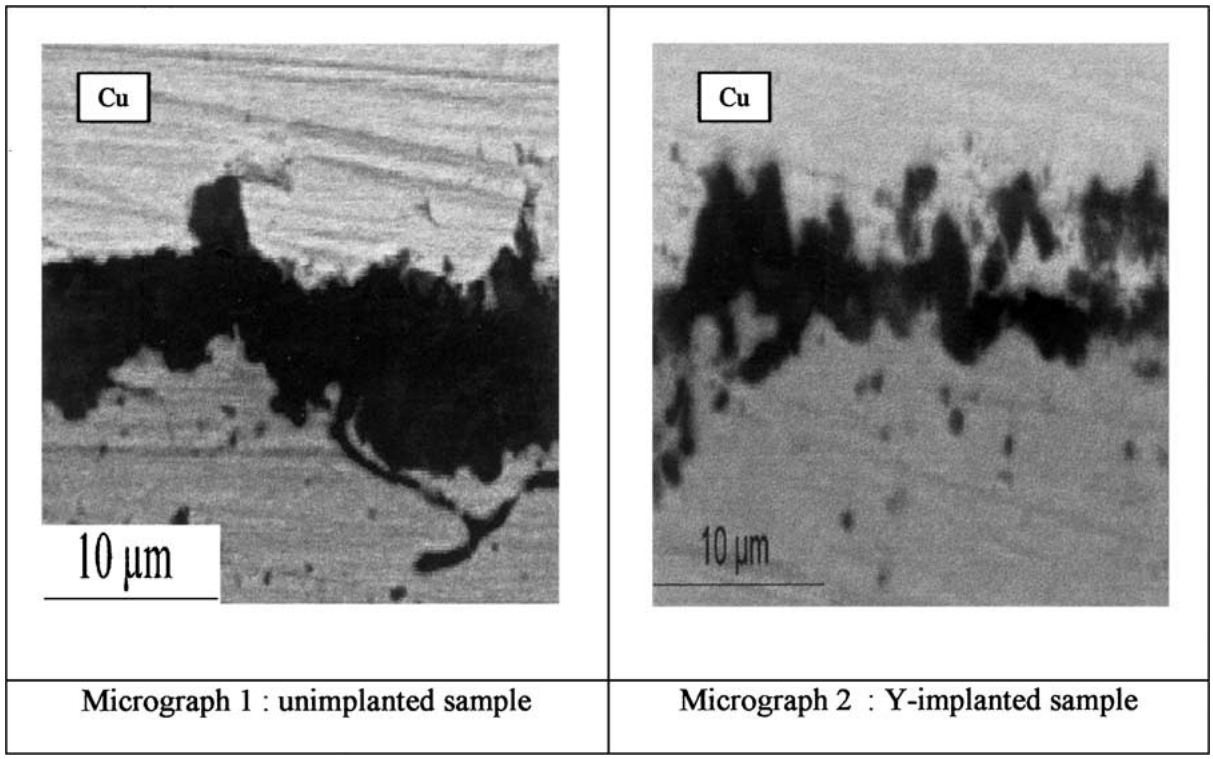

Figure 6 SEM micrographs of the cross-sections of the reference and yttrium implanted 304L stainless steel oxide scales induced after a 100-h high temperature oxidation test at 1000°C in air.

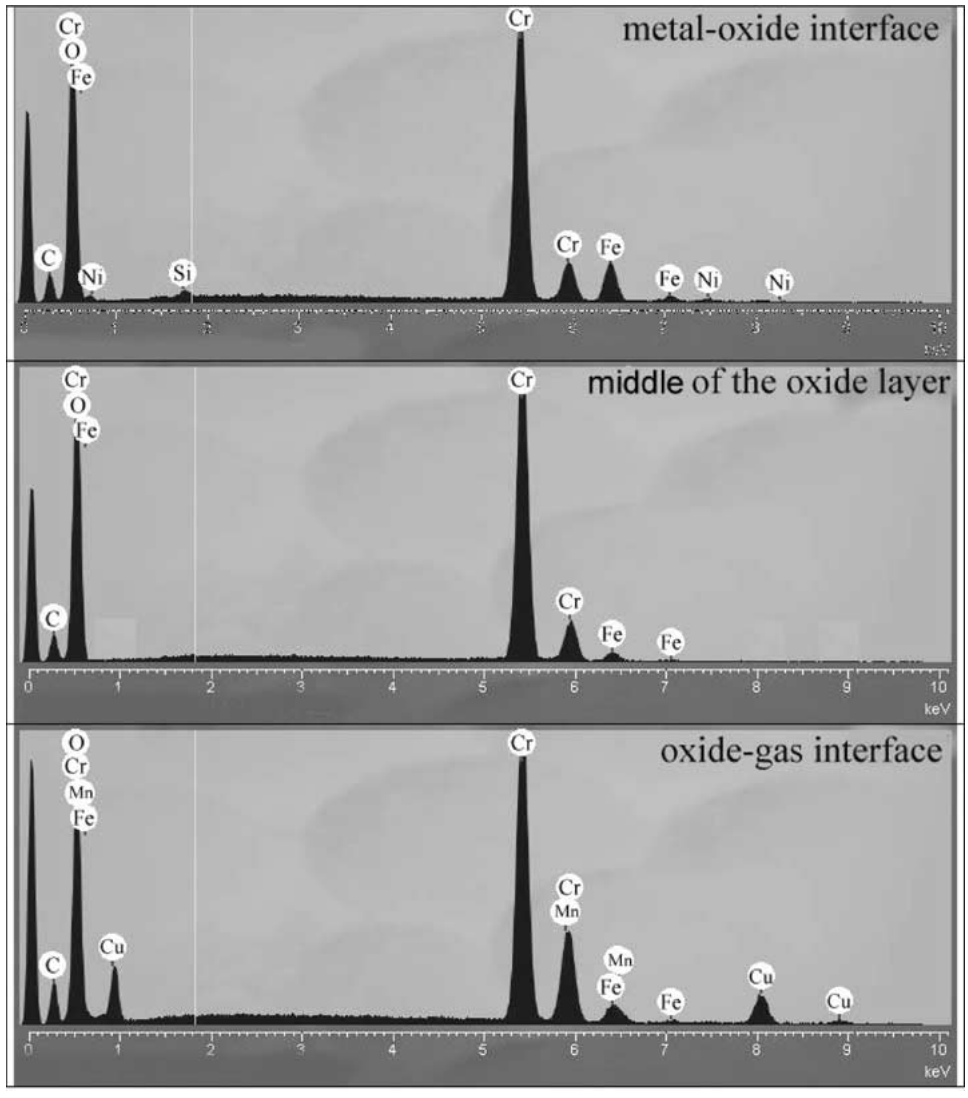

Figure 7 EDX spectra performed on the 304L reference stainless steel after a 100-h high temperature oxidation test at 1000°C in air.

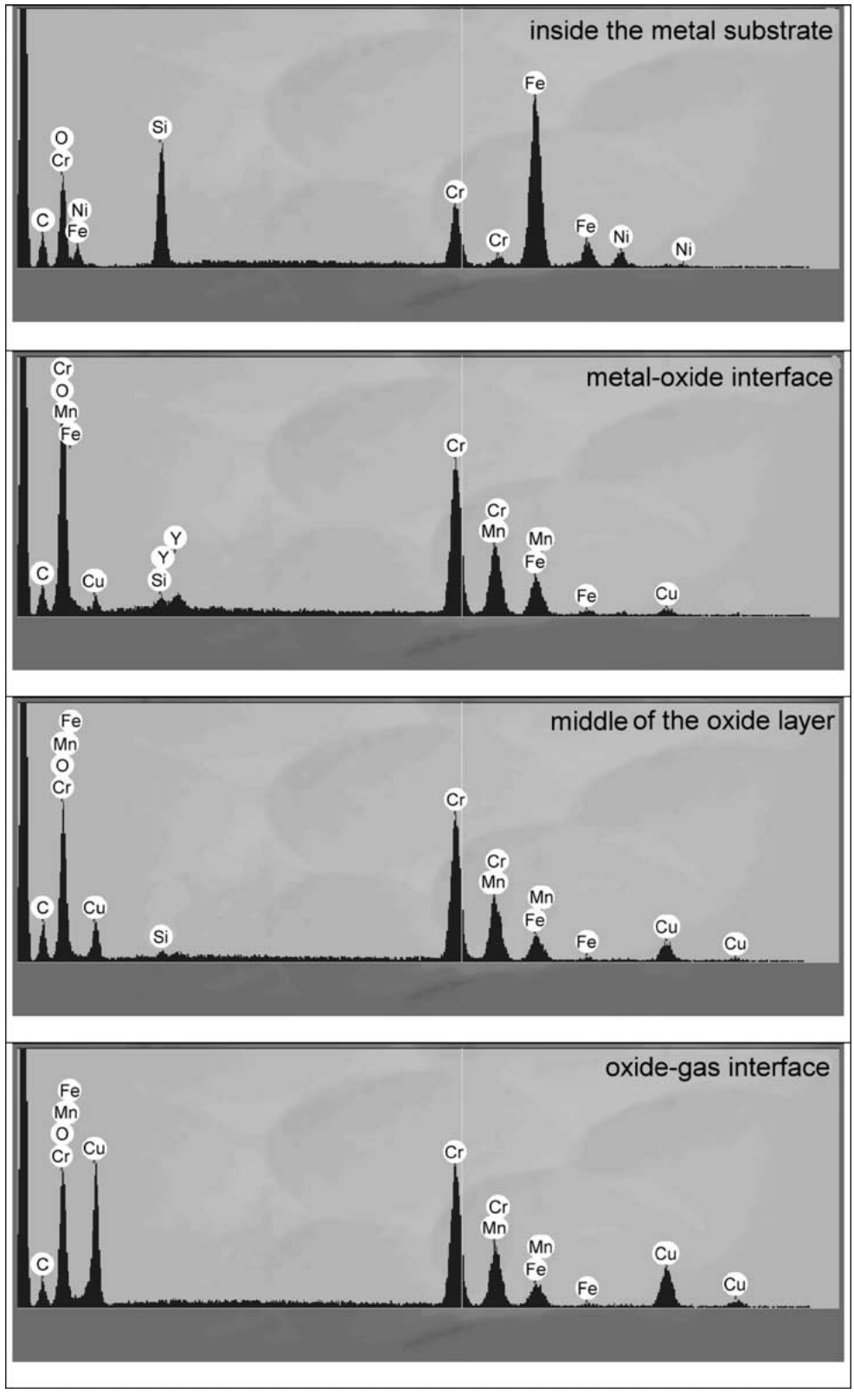

Figure 8 EDX spectra performed on the yttrium implanted 304L stainless steel after 100-h high temperature oxidation test at 1000°C in air.

stainless steel. In fact, these authors have clearly established that this silicon enrichment induces the formation of a more uniform SiO_2 layer than in the case of unimplanted AISI 304 stainless steel limiting particularly the growth of the oxide scale and the formation of iron-based oxides as observed in our study. Consequently, this oxide layer silicon enrichment induced by yttrium implantation allows also improvement of the chromia-forming stainless steel oxidation resistance at high temperature.

4. Conclusion

This study allows a better understanding of the main effects of yttrium implantation on oxidation resistance of 304L stainless steel at high temperature. In fact, yttrium implantation allows elimination of transient oxidation period observed by thermogravimetry at the beginning of unimplanted sample oxidation test and reduction of the corresponding parabolic oxidation rate. Three phenomena seem to be mainly responsible for this behavior: (a) the limitation of the iron-based oxide growths

(observed by *in situ* X-ray diffraction) in the case of unimplanted samples; (b) the yttrium localization at the metal-oxide interface (observed by EDXS) with probable segregation at the Cr_2O_3 grain boundaries inducing an inversion of the predominant diffusion mechanism and a selective chromium oxidation as observed by several authors; (c) a silicon enrichment at the metal-oxide interface (observed by EDXS) which limits the oxide scale growth and the formation of iron-based oxides. These results underline the beneficial effect of yttrium implantation which allows improvement of the oxidation resistance of commercial 304L stainless steel at high temperature.

References

1. I. M. ALLAM, D. P. WHITTLE and J. STRINGER, *Oxid. Met.* **12** (1978) 35.
2. B. A. PINT, *ibid.* **45** (1996) 1.
3. J. STRINGER, B. A. WILCOX and R. I. JAFFEE, *ibid.* **5** (1972) 11.
4. P. Y. HOU and J. STRINGER, *Mater. Sci. Eng.* A **87** (1987) 295.
5. C. M. COTELL, G. J. YUREK, R. J. HUSSEY, D. F. MITCHELL and M. J. GRAHAM, *Oxid. Met.* **34** (1990) 173.
6. K. PRZBYLSKI and G. J. YUREK, *Mat. Sci. Forum* **43** (1989) 1.
7. J. C. COLSON, H. BUSCAIL, G. BONNET, M. LACHKAR and J. P. LARPIN, *Solid State Phenomena* **41** (1985) 165.
8. M. LANDKOF, A. V. LEVY, D. H. BOONE, R. GRAY and E. YANIV, *Corros. Sci.* **41** (1985) 344.
9. J. STRINGER, *Mat. Sci. Eng.* A **120** (1989) 129.
10. R. J. HUSSEY and M. J. GRAHAM, *Oxid. Met.* **45** (1996) 349.
11. S. SEAL, S. K. BOSE and S. K. ROY, *ibid.* **41** (1994) 139.
12. A. STRAWBRIDGE and P. Y. HOU, *Mat. High Temp.* **12** (1994) 177.
13. F. H. STOTT, G. C. WOOD and J. STRINGER, *Oxid. Met.* **44** (1995) 113.
14. G. M. ECER, R. B. SINGH and G. H. MEIER, *ibid.* **18** (1982) 55.
15. E. CAUDRON, H. BUSCAIL and F. RIFFARD, *J. Mater. Sci.* **35** (2000) 3997.
16. G. SIMKOVICH, *Oxid. Met.* **44** (1995) 501.
17. M. F. STROOSNIJDER, *Surf. Coat. Tech.* **100/101** (1998) 196.
18. N. V. PLESHIVTSEV and E. A. KRASIKOV, *Russian Metallurgy Metally* **4** (1995) 64.
19. E. M. LEVIN, C. R. ROBBINS and H. F. McMURDIE, in "Phases Diagrams for Ceramists," Vol. 1 (The American Ceramist Society, 1964) p. 130.
20. M. J. CRISTÓBAL, P. N. GIBSON and M. F. STROOSNIJDER, *Corros. Sci.* **38** (1996) 805.
21. J. M. HAMPIKIAN and D. I. POTTER, *Oxid. Met.* **38** (1992) 139.
22. C. S. GIGGINS and F. S. PETTIT, *Metal. Trans.* **2** (1971) 1071.

Received 30 July 2001
and accepted 9 April 2002